Neuron
NeuroResource

Increased Brain Penetration and Potency of a Therapeutic Antibody Using a Monovalent Molecular Shuttle

Jens Niewoehner,[1] Bernd Bohrmann,[2] Ludovic Collin,[2] Eduard Urich,[2] Hadassah Sade,[1] Peter Maier,[1] Petra Rueger,[1] Jan Olaf Stracke,[1] Wilma Lau,[1] Alain C. Tissot,[1] Hansruedi Loetscher,[2] Anirvan Ghosh,[2,*] and Per-Ola Freskgård[2,*]
[1]Pharma Research and Early Development, Large Molecule Research, F. Hoffmann-La Roche, Penzberg 82377, Germany
[2]Pharma Research and Early Development, Neuroscience Discovery and Translation Area, F. Hoffmann-La Roche, Basel 4070, Switzerland
*Correspondence: anirvan.ghosh@roche.com (A.G.), per-ola.freskgard@roche.com (P.-O.F.)
http://dx.doi.org/10.1016/j.neuron.2013.10.061

SUMMARY

Although biotherapeutics have vast potential for treating brain disorders, their use has been limited due to low exposure across the blood-brain barrier (BBB). We report that by manipulating the binding mode of an antibody fragment to the transferrin receptor (TfR), we have developed a Brain Shuttle module, which can be engineered into a standard therapeutic antibody for successful BBB transcytosis. Brain Shuttle version of an anti-Aβ antibody, which uses a monovalent binding mode to the TfR, increases β-Amyloid target engagement in a mouse model of Alzheimer's disease by 55-fold compared to the parent antibody. We provide in vitro and in vivo evidence that the monovalent binding mode facilitates transcellular transport, whereas a bivalent binding mode leads to lysosome sorting. Enhanced target engagement of the Brain Shuttle module translates into a significant improvement in amyloid reduction. These findings have major implications for the development of biologics-based treatment of brain disorders.

INTRODUCTION

A major challenge to the development of biologics-based therapeutics is the inability of large molecules to effectively cross the blood-brain barrier (BBB). This poses a substantial risk to the effective development of protein and antibody-based therapies for brain disorders. For example, many of the leading therapies being developed for Alzheimer's disease rely on antibodies that target the β-amyloid protein, but only around 0.1%–0.2% of the antibody crosses into the brain (Poduslo et al., 1994). Developing effective strategies to transport large molecules across the BBB has been a long-standing goal of the field, which could transform the development of biotherapeutics for neurological and psychiatric disorders.

An attractive target for developing strategies to move molecules across the BBB has been the transferrin receptor (TfR) (Pardridge, 2012; Wang et al., 2013; Pardridge and Boado, 2012), which mediates receptor-mediated transcytosis (RMT). It has been shown that either modulating the affinity of anti-TfR antibodies or using a peptide as a transferrin ligand can improve brain exposure (Yu et al., 2011; Staquicini et al., 2011), although the increase in brain penetration is modest. We sought to investigate whether we could design a molecular shuttle (Brain Shuttle) that would effectively engage the transcytosis mechanism to enhance transport of therapeutic antibodies across the BBB and thereby achieve increased potency. We hypothesized that bivalent engagement of the TfR, as has commonly been explored, might interfere with the normal transcytosis of cargos and that monovalent binding to the receptor might engage the sorting pathway normally used to transport monomeric transferrin and lead to more efficient transport across brain endothelial cells (BECs).

We present evidence that indeed a molecular shuttle that uses monovalent binding to the TfR leads to successful transcytosis and increases brain exposure of a therapeutic antibody by well over an order of magnitude. We also provide in vivo data showing that transcellular transport occurs via vesicular structures inside the BECs. Using both mouse and human in vitro model systems, we show that bivalent binding to TfR induces lysosomal sorting and degradation consistent with the incomplete transcellular trafficking observed in vivo. In addition, bivalent receptor binding leads to a gradual downregulation of cell surface TfR because recycling of endocytosed TfR is prevented. Finally, we confirm the therapeutic potential of our approach by showing significant reduction in amyloid load in a mouse model of Alzheimer's disease.

RESULTS

Engineering of the Brain Shuttle Constructs

To test the hypothesis that mode of binding to the TfR would affect transcytosis, we engineered two different types of Brain Shuttle constructs with a single-chain (sc) Fab fragment of an anti-TfR monoclonal antibody (mAb) fused either to one or both C-terminal ends of the heavy chain of an anti-Aβ mAb (mAb31). Thus, the Fab fragment was introduced either as a single (sFab) or double (dFab) format (Figure 1A). The mAb31 used in the present study as a cargo has been shown to

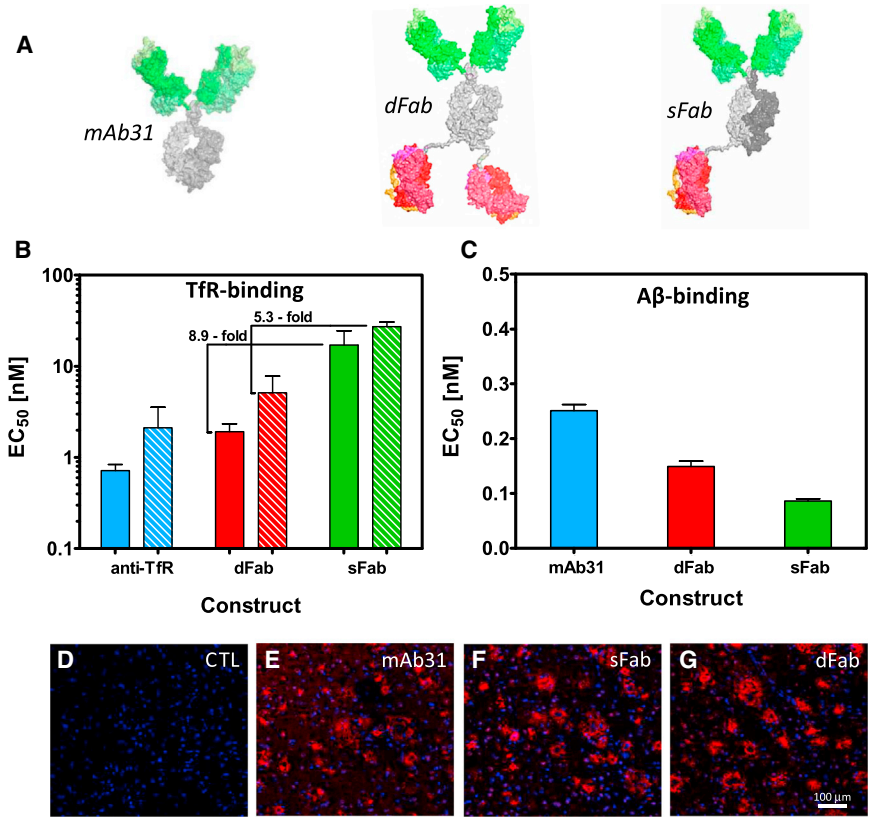

Figure 1. Schematic Representation of the Anti-Aβ mAb, Brain Shuttle Constructs, and the Antigen Binding Properties

(A) The Fab fragment (red/magenta) that binds the TfR is fused to the Fc region (gray) at the C-terminal end of an anti-Aβ mAb (mAb31) and contains either two (dFab) or one (sFab) Fab fragment. The sFab construct is produced using the knobs-into-holes approach (light- and dark-gray Fc).

(B) Indirect ELISA shows apparent affinity to TfR at two different coating densities (1 μg/ml mTfR solid; 0.5 μg/ml mTfR stippled) for the original anti-TfR IgG format and the two Brain Shuttle constructs. The sFab shows a slight reduction in apparent affinity compared to dFab (5.3- to 8.9-fold dependent on coating density) due to loss in avidity.

(C) ELISA displays the apparent binding affinity to immobilized β-amyloid fibrils of the parent mAb31, dFab, and sFab constructs. All constructs show comparable high-affinity binding (between 0.25 and 0.09 nM).

(D–G) Cryosections from 12-month-old PS2APP transgenic mice were stained with the following constructs: (D) control using only the secondary detection antibody, (E) mAb31, (F) sFab, and (G) dFab. All constructs bind equally well to β-amyloid plaques in PS2APP transgenic animals. CTL, control where no antibody construct has been added to check for background signal.

Data are presented as mean ± SD. See also Figure S1.

specifically bind with high affinity to β-amyloid plaques (Bohrmann et al., 2012). The sFab format was produced to mimic the monovalent binding mode of the natural ligand transferrin, and the dFab represents a standard IgG configuration, whereas flexible linkers were used instead of the IgG-hinge regions. Importantly, none of the Brain Shuttle constructs competes with the binding of transferrin to the TfR (Figure S1 available online). The antigen affinity of the constructs was measured in an ELISA setup against mouse TfR (mTfR) and human Aβ peptide. The binding properties toward the TfR were preserved in the two Brain Shuttle constructs. As expected, the sFab apparent binding affinity was slightly reduced (5.3- to 8.9-fold) when compared to the dFab construct and was dependent on TfR-coating density (Figure 1B). The Aβ apparent binding properties were also preserved in the two Brain Shuttle constructs showing subnanomolar binding as the parent antibody mAb31 (Figure 1C). In addition, plaque binding on brain tissues from PS2APP transgenic animals was also maintained (Figures 1D–1G). Epitope mapping of the anti-TfR mAb (Figure S1) shows that the Brain Shuttle module binds at the apical domain of TfR, which is distant to the binding site of transferrin.

Receptor Binding Mode Determines TfR Cellular Trafficking within BECs

We used a BEC system (bEnd3 cells) to investigate the intracellular sorting of the sFab and dFab constructs. Previous studies by Lesley et al. (1989) and Crépin et al. (2010) had indicated that expression and intracellular sorting of TfR were directly affected by valency of the ligand. We exposed BECs with sFab or dFab at equal concentration for 1 hr to allow TfR binding, internalization, and intracellular sorting. FACS analysis indicated that the dFab construct was more rapidly internalized (Figure 2A), and this was confirmed by immunocytochemistry (Figures 2B–2D). Notably, the high level of colocalization of the dFab construct with the lysosome-associated membrane protein Lamp2 suggests significant intracellular sorting of the dFab construct to the lysosome (Figure 2E). We found that >50% of vesicular structures positive for Lamp2 also contained the dFab construct. In contrast to the dFab construct, significantly less lysosomal colocalization was seen for the sFab construct, suggesting that the mode of binding to TfR affected intracellular sorting.

To determine if there was a difference in the rate at which the sFab and dFab constructs were recycled to the surface, we treated cells with bafilomycin A1 (BafA1), which is known to inhibit recycling of transferrin (Michel et al., 2013; Kozik et al., 2013). BafA1 treatment led to a strong increase in cellular accumulation of the sFab (Figure S2), indicating that the sFab construct is normally recycled back to the cell surface, whereas the dFab construct showed defective recycling even without BafA1 treatment. If the bivalent receptor binding mode of the dFab construct induces sorting of the construct to the lysosome, one would expect that cellular TfR levels would be affected when exposed to dFab. Consistent with this prediction, exposure of the BECs to the dFab construct significantly decreased cell surface TfR to almost nondetectable levels (Figure 2F). In contrast,

the sFab construct had no detectable effect on cell surface expression levels of TfR (Figure 2F), indicating that the monovalent binding mode of sFab does not disturb the cellular TfR homeostasis. We also performed intra- and extracellular staining of TfR using FACS. Again, we observed downregulation of cell surface TfR at an early time point, but the total cell TfR was not affected (Figure 2G). However, after 24 hr exposure to the dFab construct, the internalized fraction of TfR was no longer detectable, likely due to lysosomal degradation. dFab-induced degradation of the TfR was confirmed by analyzing protein levels using western blot (Figure S3).

We sought to confirm our observations in a BBB transcytosis assay using the well-characterized human BEC line hCMEC/D3 (Weksler et al., 2005). Because the anti-TfR Fab fragment used in the experiments described above is not cross-reactive with human TfR, mono- and bivalent antibody constructs binding to human TfR were generated and tested in a standard transwell setup (Figure 2H). Because hCMEC/D3 cells are known to form leaky tight junctions (Weksler et al., 2005), the assay was performed in a pulse-chase mode to avoid assay disturbance by paracellular flux. The monovalent (Figure 2I) or bivalent (Figure 2J) antibodies were added in the upper chamber to allow internalization promoted by the TfR expressed on the apical surface of the hCMEC/D3 cells. After receptor-mediated uptake for 1 hr, the upper and lower chambers were washed, and the amount of construct in the upper and lower chambers as well as inside the BECs was quantified over time. Only the monovalent antibody could be detected in the lower chamber, whereas the bivalent antibody was not detected. These experiments, using a different mono-/bivalent TfR antibody pair with specificity for human TfR, confirm our previous findings in a murine system and indicate that receptor binding mode determines efficiency of transcytosis. Importantly, the monovalent TfR antibody specific for human TfR, which shows transcytosis activity, has comparable apparent affinity (EC_{50}, 3.8 nM) to the dFab construct (EC_{50}, 6.4 nM), which is incapable of crossing the BBB (both EC_{50} values determined by FACS). This suggests that the monovalent binding mode to the TfR, and not just reduced affinity, is the key factor for efficient transcytosis. Interestingly, this human-specific antibody binds to a similar region on the apical domain of the TfR as the mouse-specific antibody (Figure S1).

In the next series of experiments, we wanted to determine if the sFab and dFab constructs behave differently when engaging with the TfR on the BBB in vivo. To investigate the transport process, we used the well-characterized PS2APP double-transgenic mouse model of amyloidosis (Richards et al., 2003) in which the quantification of amyloid plaque-bound mAb31 enabled us to directly measure target occupancy in the brain. We first studied the rate of BBB crossing shortly after injection of equimolar amounts of the two Brain Shuttle constructs. At 15 min after intravenous (i.v.) injection, there was a substantial uptake into brain microvessels of both the sFab and dFab constructs (Figures 3A, 3B, and 3F). However, at 8 hr postinjection, we observed a striking difference in the distributions of the sFab and dFab constructs. Whereas the sFab construct concentration was significantly reduced in the capillaries and highly associated with amyloid plaques (Figure 3C; higher magnification shown in Figure 3G), the dFab construct was only detectable within the microvascular structures (Figure 3D), suggesting that the sFab construct was more efficient in crossing from the blood vessels to the brain parenchyma. Quantification of these data confirmed that reduction of construct localization in the microvessels correlates with an increase in plaque decoration for sFab due to the extensive transport of the construct into the CNS compartment (Figures 3E and 3G). Taken together, these data suggest that the TfR binding mode of the constructs determines the rate and extent of transcytosis and thus the degree of brain exposure. These imaging data, where we detect the construct using fluorescence intensity, were confirmed by measuring the concentration of the constructs in total brain and brain blood vessels in both transgenic and wild-type animals (Figure S4). Again, we detected much higher levels of the sFab in total brain compared to dFab and much more dFab accumulation in the capillary fraction. The data are very similar in both transgenic and wild-type animals except that the sFab concentration is higher in transgenic animals than the wild-type 24 hr postinjection. This sustained concentration for sFab in transgenic animals could be due to the intensive target engagement seen using the imaging approach.

To further investigate how the mode of receptor binding affects sorting of constructs in vivo, we used high-resolution confocal imaging to elucidate the difference between the sFab and dFab construct behavior at the BBB. Specific markers for the luminal side (podocalyxin) and abluminal side (collagen IV) (Figure 4A) of the microvessels were used to identify the BEC intracellular space (arrow in Figure 4B). Within 15 min postinjection, the sFab construct could be identified in granular structures inside the BECs (Figure 4C; Movie S1). One possibility is that these granular structures containing the sFab construct are TfR-containing early endosomes formed by clathrin-mediated endocytosis. Furthermore, by analyzing microvessel cross-sections, we were able to identify the sFab and dFab constructs internalized into the BECs based on costaining with the luminal marker podocalyxin (Figures 4D and 4F). By 8 hr postinjection, the staining for sFab construct was reduced, whereas substantial staining was still observed for the dFab construct (Figures 4E and 4G). These data are in agreement with the microvessel quantification data (Figure 3G). We also investigated the localization of sFab and dFab constructs in relation to the abluminal side by costaining with collagen IV 8 hr postinjection. For the sFab construct, there was a clear overlap with the abluminal marker and frequent staining signals in the brain reflecting binding to parenchymal amyloid deposits (Figures 4H–4K). In contrast, the dFab staining was only detected inside the BECs and not in direct contact with the abluminal side (Figures 4L–4O). This is in agreement with earlier studies showing no or only minor colocalization of an anti-TfR antibody with laminin (Gosk et al., 2004) and collagen IV after i.v. injection (Paris-Robidas et al., 2011). Thus, the failure of dFab constructs to cross the BBB is associated with their inability to reach the abluminal side for a productive release. Costaining with a lysosomal marker (Lamp2) indicated that the dFab construct was present in lysosomal compartments in vivo (Figure 4P). By analyzing the intensity profiles corresponding to dFab and Lamp2 signals, we found perfect colocalization and that the dFab granule of 350 nm in diameter is contained within a 500 nm Lamp2-positive lysosome

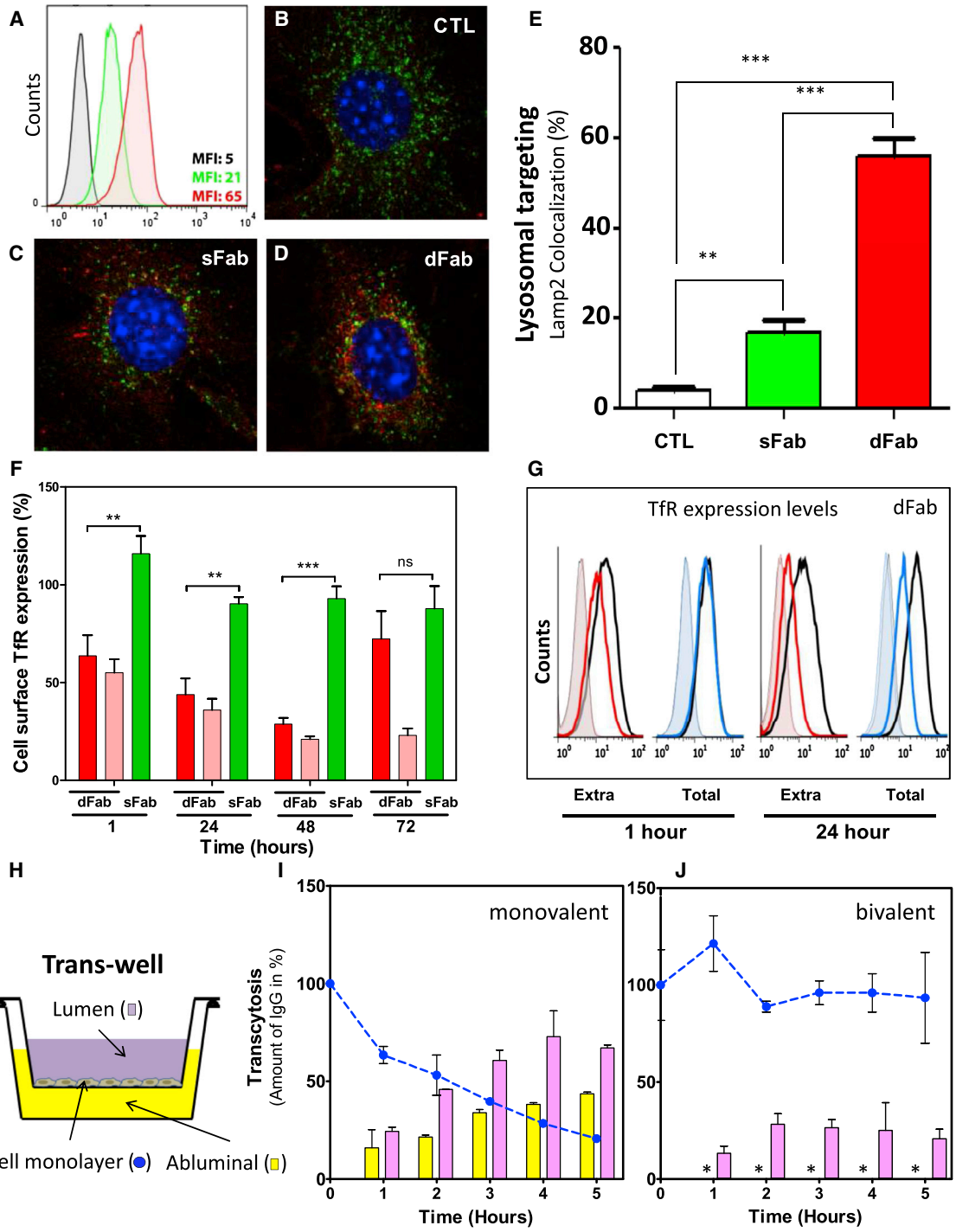

Figure 2. Influence on TfR Intracellular Sorting, Cellular Trafficking, and Transcytosis Activity in BECs

(A) Uptake of sFab (green) and dFab (red) by intracellular FACS is presented. MFI, mean fluorescence intensity.

(B–D) Immunocytochemistry on bEnd3 cells for control (B), sFab (C), and dFab (D) constructs is shown in red and lysosomes (Lamp2) in green.

(E) Percentage of lysosomal colocalization after 1 hr uptake is shown. More than 50% of lysosomes contain dFab, whereas less than 20% contain sFab construct. CTL, control where no antibody construct has been added to check for background signal.

(F) Time- and dose-dependent downregulation of cell surface TfR by dFab at 2.5 μg/ml (red) and 25 μg/ml (pink) is shown. For the sFab construct at 2.5 μg/ml (green), no significant changes were detected.

(G) Extracellular (red) and total (blue) TfR expression after 1 hr exposure to 2.5 μg/ml dFab leads to cell surface downregulation, but total cell receptor expression is unaffected. After 24 hr exposure to 2.5 μg/ml dFab, further downregulation of cell surface TfR expression and also intracellular reduction are shown. Isotype control and nontreated cells (black) are shown in comparison.

(legend continued on next page)

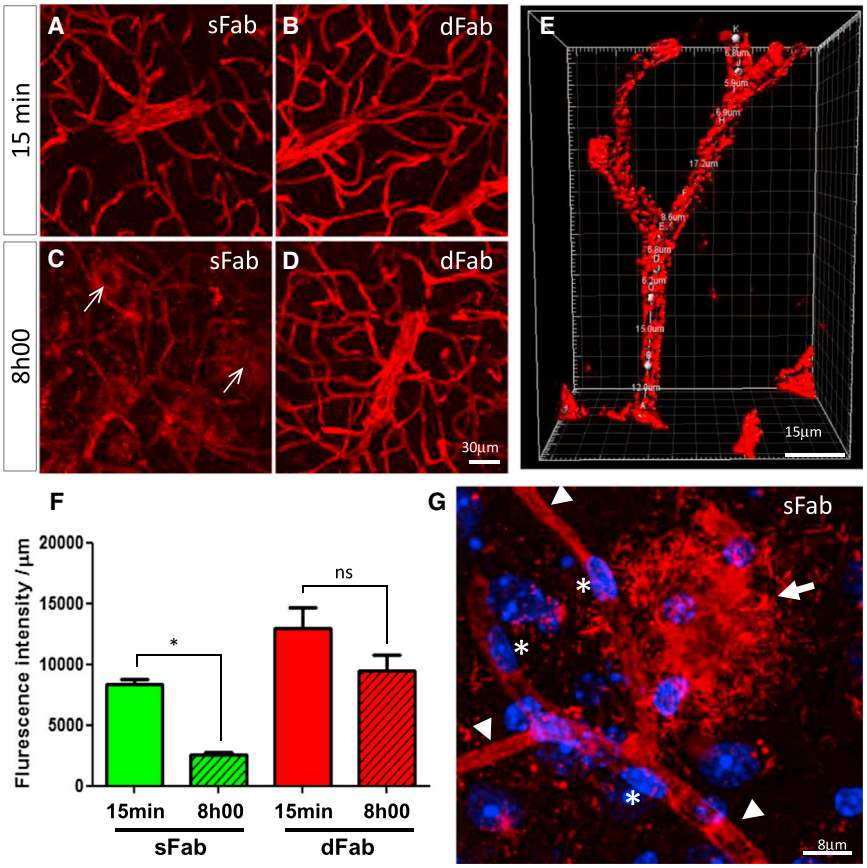

Figure 3. Brain Microvessel Targeting and Parenchymal Exposure of dFab and sFab Constructs in the PS2APP Transgenic Mouse Model

PS2APP animals treated with equimolar concentrations of dFab (16.7 mg/kg) and sFab (13.3 mg/kg) were perfused, fixed, and processed for immunostaining.

(A and B) Extensive accumulation of both sFab (A) and dFab (B) inside BECs 15 min postinjection is shown.

(C and D) Eight hours postinjection, the sFab (C) escapes the microvessels into the parenchyma space and decorates β-amyloid plaques (arrows). dFab at 8 hr postinjection (D) remains in the microvessels, and no β-amyloid plaque decoration is detectable. Confocal settings from the dFab 8 hr sample were used for all images in (A)–(D).

(E) The amount of sFab and dFab was quantified by fluorescence intensity within well-defined brain microvessels.

(F) Quantification shows that both constructs accumulate rapidly (dFab somewhat faster) within the BECs, but only the sFab construct is able to escape the microvessels 8 hr postinjection. *p ≤ 0.05.

(G) A magnified image shows an amyloid plaque structure decorated with sFab 8 hr postinjection (arrow) and the capillaries (arrowheads). Asterisks indicate the BEC nucleus.

Data are presented as mean ± SD.

(Figure S5). These data are in agreement with our in vitro cell culture findings and indicate that dFab constructs are targeted for lysosomal degradation, which is likely the reason for the lack of transcytosis.

Monovalent Receptor Binding Mode Is Crucial for Transporting Cargo across the BBB

The anti-Aβ mAb mAb31 is a very specific and potent Aβ plaque binder (Bohrmann et al., 2012), providing us with a powerful readout to quantify target engagement within brain parenchyma. We used the PS2APP double-transgenic amyloidosis model (Richards et al., 2003) to investigate the amount of brain exposure of the two Brain Shuttle constructs compared to the mAb31 parent antibody. The three variants were injected i.v. at equimolar concentrations, and the degree of brain exposure was determined by quantifying the amount of antibody present at plaques 8 hr postinjection. For the dFab construct, no significant increase in plaque decoration was detected compared to mAb31 (Figure 5A). However, for the sFab construct, there was a massive increase in plaque decoration in comparison with the parent mAb31 antibody. These data are in agreement when directly measuring the concentration of the constructs with an immunoassay (Figure S4). Target engagement at the amyloid plaques was improved more than 50-fold for the sFab construct based on fluorescence intensity quantification using a labeled secondary antibody. Whereas the sFab construct showed extensive plaque decoration (Figure 5D), the dFab was only detectable in the microvessels (Figure 5C), indicating that the dFab construct targets and enters brain microvessels but fails to escape at the abluminal side. The sFab construct does not disrupt the BBB as a mechanism for antibody uptake into the brain because there was no significant increase in Evans blue leakage when animals were dosed with the sFab construct (Figure S6).

We investigated the target engagement capacity of the sFab construct at a low dose of 2.66 mg/kg and prolonged in vivo exposure time up to 7 days. Maximal plaque decoration was reached within 8 hr, followed by persistent plaque binding over at least 1 week after a single injection (Figure 5E). In a previous study, the parent mAb31 had been shown to reach maximal plaque binding 7 days after injection (Bohrmann et al., 2012). Quantification of the staining in microvessel structures indicated

(H) Transcytosis activity of mono- and bivalent antibody constructs against human TfR was measured in vitro using human BECs. The construct concentration was determined at the luminal side (magenta), abluminal side (yellow), and intracellular space (blue).

(I and J) The monovalent IgG construct was transported to the abluminal side (I, yellow), whereas the bivalent IgG construct was not detectable at the abluminal side (J).

Data are presented as mean ± SD. *p ≤ 0.05, **p ≤ 0.01, and ***p ≤ 0.001. ns, not significant. See also Figures S2 and S3.

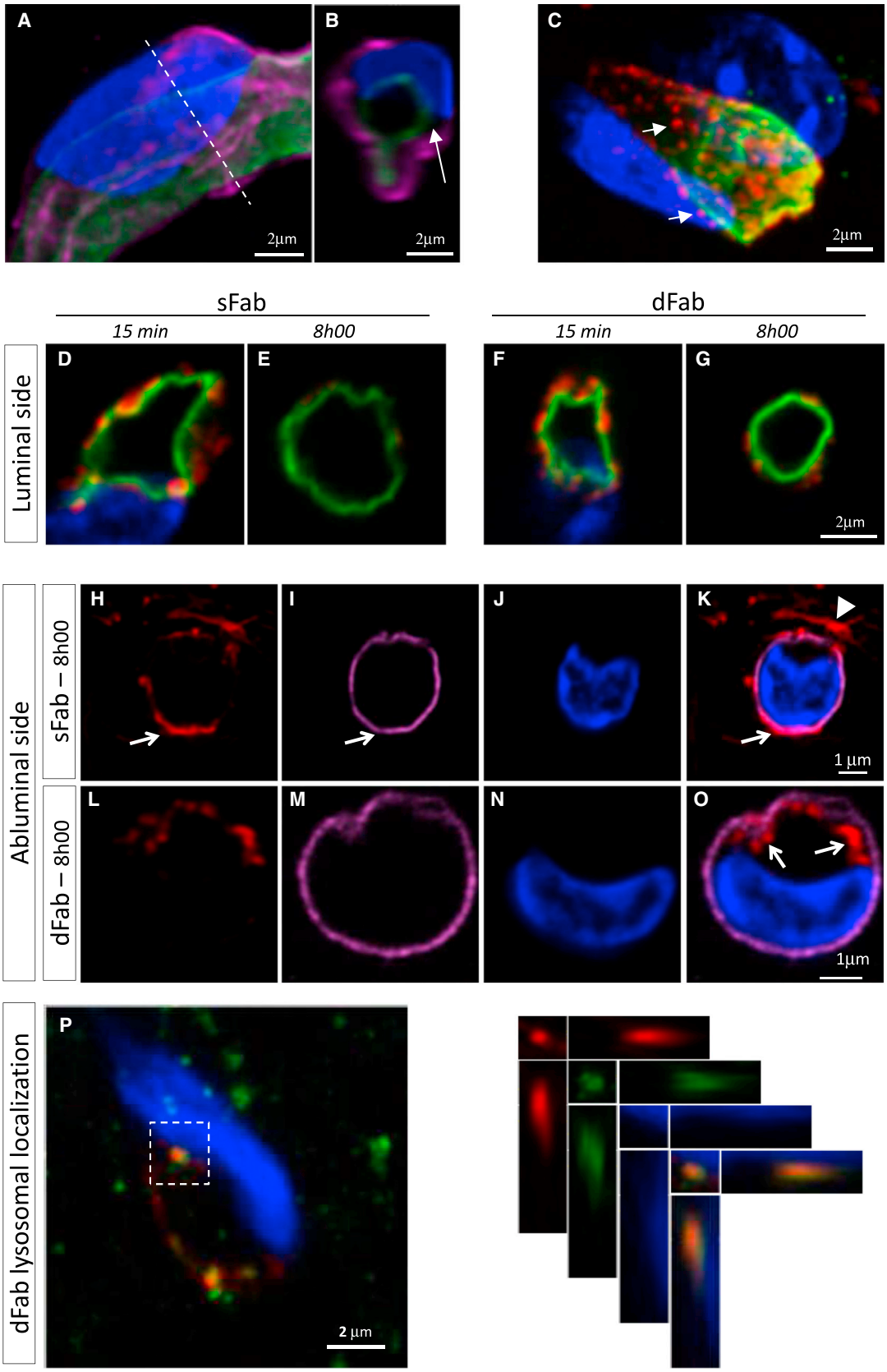

(legend on next page)

that the localization of the sFab construct was very transient at the BBB, illustrating the relatively rapid rate at which the construct crosses the barrier (data not shown). The representative plaque-staining images for the parent antibody mAb31 at 2 mg/kg 7 days postinjection (Figure 5F) and equimolar concentration for the sFab construct (Figure 5G) illustrate the increase in plaque binding one achieves with the sFab Brain Shuttle construct. The sFab construct shows only a minor colocalization with the lysosomal compartment, which likely reflects normal constitutive trafficking of the TfR to the lysosome (Matsui et al., 2011). Our in vitro studies also showed recycling and transcytosis of the sFab construct. Taken together, these findings suggest that the sFab construct does not interfere with the normal trafficking of the TfR. In contrast, the dFab construct shows strong colocalization with the lysosomal compartment but no transcytosis activity, neither in vitro nor in vivo. These findings are captured in a simplified model (Figure 5H), which illustrates the difference in intracellular trafficking inside the BECs between sFab and dFab constructs and its comparison with the natural ligand transferrin.

Increased Antibody Delivery across the BBB Translates into Enhanced In Vivo Potency

In the final set of experiments, we asked whether the significant increase in brain exposure using a monovalent binding mode improves in vivo potency of the anti-Aβ antibody in a long-term treatment study. Because there is no detectable plaque target engagement of the dFab (Figure S7) even at a high dose (17.44 mg/kg) 7 days postinjection, we did not include this construct in further in vivo potency investigations. The sFab construct was compared to the parent mAb31 antibody, which shows some target engagement at the equimolar dose level (10 mg/kg). For this experiment, we injected the sFab construct and the control parent antibody mAb31 weekly for 3 months. In a previous 5-month study, the therapeutic antibody mAb31 had been shown to reduce the plaque burden at 20 mg/kg (Bohrmann et al., 2012). Based on the data shown in Figure 5, we selected two low doses to investigate if improved brain exposure would lead to enhanced in vivo potency. Target plaque binding at the end indicated that at both doses, there was stronger target engagement with the sFab construct than the parent mAb31 antibody (Figures 6A–6D). The degree of amyloidosis in the APPPS2 double-transgenic mice was quantified at baseline, and following vehicle, low-dose parent mAb31 and low-dose sFab construct treatment (Figures 6E–6H). At these low doses, no in vivo effect was detected with the parent mAb31 (Figure 6I), which was anticipated based on a previous long-term study over 5 months (Bohrmann et al., 2012). In contrast, a significant reduction in plaque numbers both in cortex and hippocampus was observed with the middose of 2.67 mg/kg of the sFab construct. Even at the much lower dose of 0.53 mg/kg (Figure 6I), a trend was seen in favor of the sFab construct, especially in the cortex, although it did not reach statistical significance. A secondary analysis of plaque sizes revealed a more pronounced reduction of numbers for small plaques (Figure S8), in agreement with the mode of action for mAb31 (Bohrmann et al., 2012). These data indicate that increased brain penetration, enabled by a monovalent mode of TfR binding, leads to a significant improvement in the potency of a therapeutic antibody in a chronic animal model of Alzheimer's disease pathology.

DISCUSSION

Engagement of the TfR has been used in previous studies as an approach to facilitate the movement of large molecules across the BBB, but in most cases, the level of transcytosis has been modest, and there has been limited understanding of the determinants of effective transport (Wang et al., 2013; Yu et al., 2011; Staquicini et al., 2011; Sumbria et al., 2013). Although recent studies focused on the effect of antibody affinity to the efficiency of transport (Yu et al., 2011), we explored the hypothesis that monovalent versus bivalent engagement of the TfR may be a much more important determinant of transport efficiency. Consistent with this hypothesis, our experiments show that the binding mode to the TfR is absolutely crucial for successful transport of antibodies across the BBB. We also find that increased brain exposure is associated with a considerable increase in potency for a therapeutic antibody in a chronic model of Alzheimer's disease (Figure 6). Our findings imply significantly improved treatment options for early disease modification in preclinical Alzheimer's disease in general and, in particular, in ApoE4 gene carriers being at higher risk of developing Alzheimer's disease (Mielke et al., 2012). The difference in brain exposure between a bivalent and monovalent binding mode is striking. Our imaging experiments show extensive uptake of both sFab and dFab construct in brain capillaries within minutes

Figure 4. High-Resolution Imaging of Brain Microvascular Structure Identifies the Brain Shuttle Constructs within BECs at the BBB

PS2APP animals were treated with the constructs as described in Figure 3.

(A) 3D reconstruction of a microvessel using antibodies rise against the luminal (podocalyxin; green) and the abluminal (collagen IV; magenta) sides of the microvessel. The nucleus of the endothelial cell is depicted in blue (DAPI). Dashed line is cross-section line for the image in (B).

(B) Cross-section of the image displayed in (A) is shown where the arrow indicates the BEC intracellular space.

(C) A microvessel with the luminal side (podocalyxin, green) and the sFab construct (red) 15 min postinjection shows the construct within vesicular structures inside the BECs, clearly illustrated in Movie S1.

(D–G) Subcellular localization of sFab (D and E) and dFab (F and G) in microvessel 15 min (D and F) and 8 hr (E and G) postinjection is shown. (D)–(G) were acquired with the same confocal settings. Construct is shown in red and the luminal membrane (podocalyxin) in green.

(H–K) sFab (red) crosses the basal lamina (collagen IV, magenta) of the microvessels 8 hr postinjection. (K) Merged image shows costaining at basal lamina (arrow) and sFab-positive plaques around the microvessel (arrowhead).

(L–O) dFab (red) does not reach the abluminal side (collagen IV, magenta) 8 hr postinjection. (O) Merge image shows intracellular staining of dFab (arrows).

(P) dFab (red) colocalized with Lamp2-positive lysosomes (green), suggesting sorting to the degradation pathway in vivo. XYZ stack of the boxed area shows that the dFab construct (red) accumulates within a Lamp2-positive lysosome (green).

See also Figure S5.

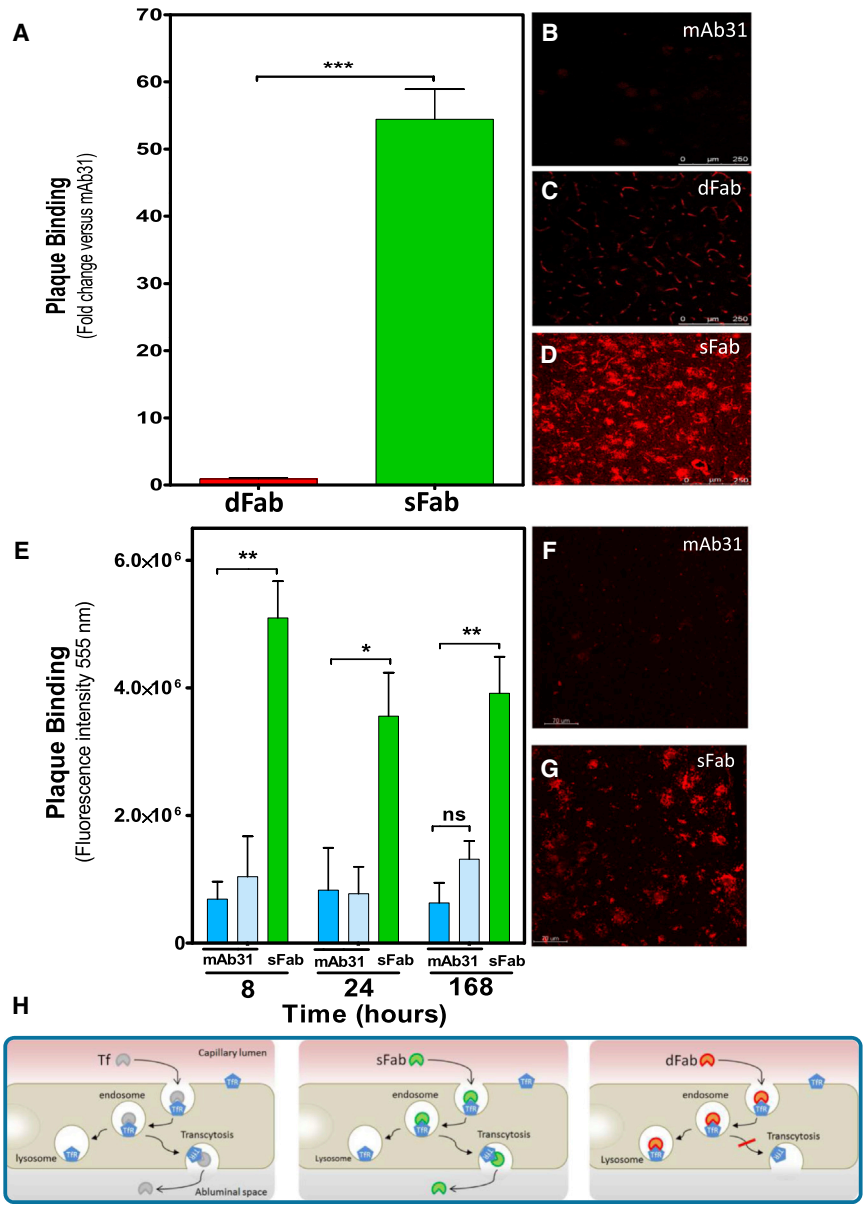

Figure 5. Brain Exposure and Plaque Decoration after i.v. Administration

(A) mAb31 (10 mg/kg), dFab (16.7 mg/kg), and sFab (13.3 mg/kg) constructs were i.v. injected in PS2APP transgenic animals at equimolar concentrations, and animals were perfused and sacrificed 8 hr postinjection. No significant increase in plaque decoration was detected for the dFab compared to mAb31. For the sFab construct, a 55-fold higher plaque decoration was detected than the parent mAb31 based on fluorescence intensity at 555 nm from the detection antibody.

(B–D) Representative immunohistochemistry staining in the cortex of mAb31 (B), dFab (C), and sFab (D) 8 hr postinjection is shown. The dFab shows only microvessel staining, whereas the sFab decorates the β-amyloid plaques extensively.

(E) Graph shows that a low dose of the sFab construct (green, 2.66 mg/kg) rapidly and significantly reaches the plaques in the brain compared to both 2 mg/kg (blue) and 10 mg/kg (light blue) of mAb31. The target engagement of the sFab construct is sustained over at least 1 week postinjection.

(F and G) Immunohistochemistry staining shows plaque decoration for mAb31 at 2 mg/kg (F) and sFab at 2.66 mg/kg (G) 7 days postinjection.

(H) Simplified model illustrates the difference in intracellular sorting of Tf, sFab, and dFab. Both Tf and sFab are able to cross the BECs by preserving TfR's natural intracellular trafficking. In contrast, dFab induces an abnormal configuration of TfR leading to lysosomal sorting and degradation.

Data are presented as mean ± SD. See also Figure S4.

after injection (Figure 3), but the fate of sFab and dFab cargos diverges after that. Whereas the sFab construct exits the capillaries, enters the CNS compartment, and efficiently engages the target, the dFab constructs remain within BECs and become colocalized with lysosomal markers, suggesting sorting into a degradation pathway.

The precise mechanism by which the sFab construct escapes lysosomal sorting and is released on the abluminal side is not known. It could be that the sFab construct simply docks as an additional ligand onto the TfR adjacent to transferrin without changing the way the receptor complex is recognized by the intracellular-sorting machinery. Thus, sFab constructs may efficiently use the endogenous transcytosis mechanism to get across the BECs. In contrast, the dFab constructs may induce substantial dimerization of the TfR, followed by internalization and sorting to a lysosomal pathway. This could potentially be prevented using a low-affinity dFab variant to reduce dimerization of TfR on the cell surface or inside specific organelles. Different subpopulations of TfR-containing early endosomes have been described, raising the possibility that different internalization mechanisms could deliver cargo into different subsets of early endosomes (Navaroli et al., 2012). Local clustering of TfR on the cell surface using multivalent streptavidin increases the rate of endocytosis primarily due to enhanced clathrin-coated pit initiation (Liu et al., 2010). Pre-early endosome sorting has been shown to begin at the plasma membrane (Lakadamyali et al., 2006). Under these conditions, dynamic endosomes could be formed leading to degradation of the cargo, which may be the mechanism that targets dFab constructs to the lysosome. Whether these different modes of internalization are involved in discrimination between the sFab and dFab needs to be further investigated, but our data strongly suggest that differences in TfR binding mode lead to major differences in intracellular sorting, which ultimately allows sFab-associated cargos to cross the BBB.

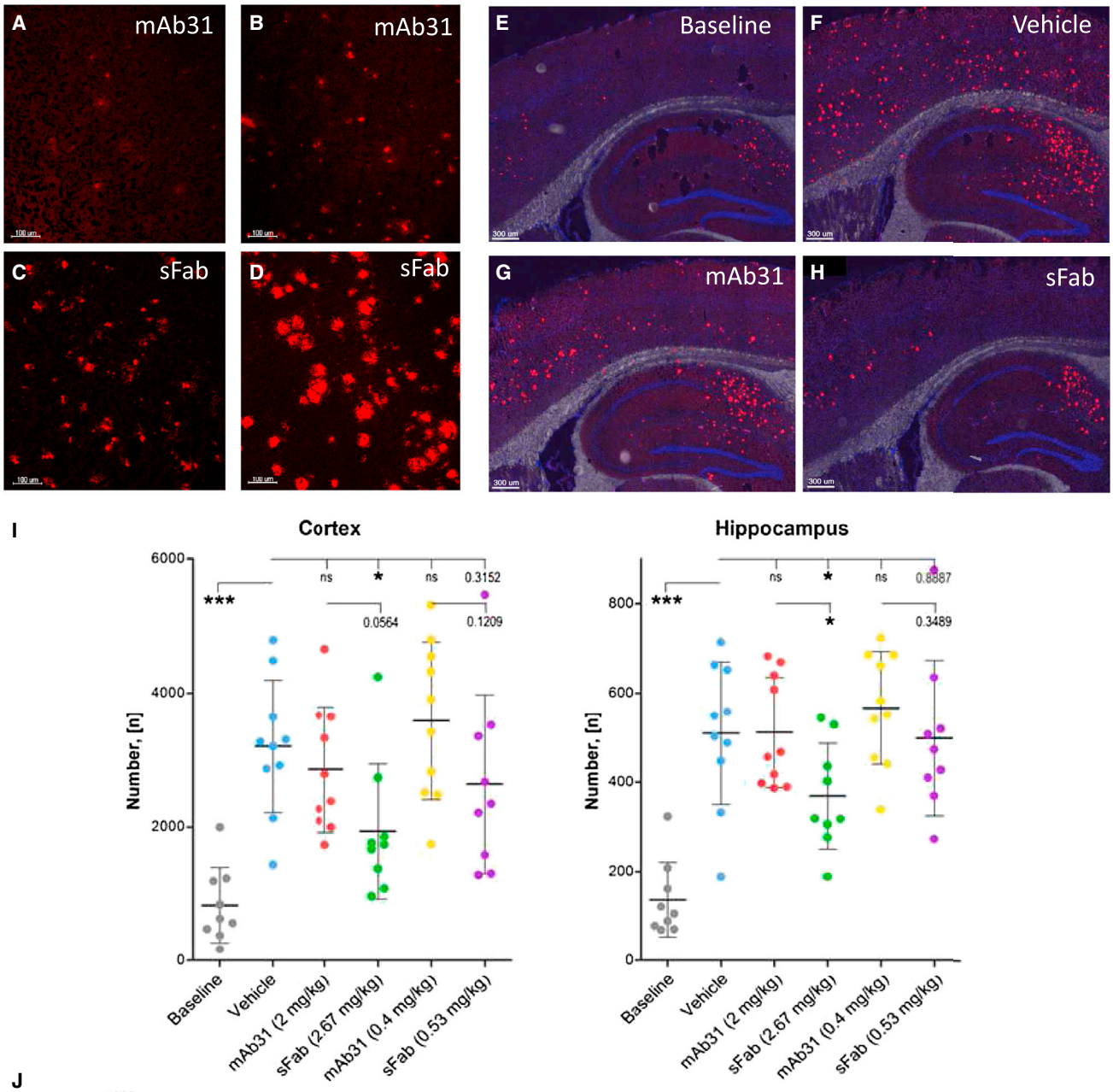

(legend on next page)

Our data also indicate that bivalent TfR binding could have a significant effect on receptor function. As shown in Figure 2, prolonged in vivo exposure with a bivalent, and likely also with a multivalent, construct can lead to downregulation of cell surface TfR, which might impact the survival of cell populations relying on iron uptake, e.g., erythrocyte precursors. TfR is involved in regulation of iron homeostasis associated with adult neurodegeneration (LaVaute et al., 2001), and TfR knockout mice show defects in nervous and hematopoietic systems (Levy et al., 1999). Thus, the design of novel Brain Shuttle constructs should start with an understanding of the underlying BBB receptor biology in order to generate variants that are both efficient in crossing the BBB and have an acceptable safety profile. Our Brain Shuttle design with a sFab fragment fused to the C-terminal end of the Fc domain preserves the normal IgG structure of the therapeutic antibody while greatly increasing the delivery of the antibody to the brain parenchyma. Such a Brain Shuttle design could be expanded to other cargos, such as therapeutic growth factors, enzymes, and peptides, and could greatly facilitate the development of a new generation of biotherapeutics for brain disorders.

EXPERIMENTAL PROCEDURES

Engineering of Brain Shuttle Constructs

Brain shuttle constructs were engineered by fusing a sc Fab fragment of an antibody against the mTfR raised in rats to the C terminus of the heavy chain of an antibody against Aβ (mAb31). Although mAb31 is a humanized antibody, the sc Fab fragment contained human constant and rat variable regions, connected by a glycine-serine linker. In the case of the monovalent construct, knobs-into-holes technology was used to favor heterodimeric pairing of one mAb31 heavy chain carrying the mTfR antibody fragment to a "free" heavy chain. For the in vitro transcytosis assay, an antibody against the human TfR was generated either as a standard IgG or in a "one-armed" IgG format using knobs-into-holes.

Immunohistochemistry, Immunocytochemistry, Image Processing, and Quantification

All animal studies were performed according to Roche animal license. Six-month-old PS2APP transgenic mice were i.v. injected with sFab or dFab-mAb31 constructs (10 mg/kg). At 15 min or 8 hr postinjection, animals were anesthetized, transcardially perfused with 1× PBS, followed by 2% paraformaldehyde. The perfused brains were soaked in 2% paraformaldehyde for 7 hr before sectioning. After inclusion in agarose, brains were cut using a Leica VT1000M vibratome at 100 μm in the sagittal plane. Sections were stored at −20°C in 1× PBS/glycerol (1/1). For the immunostaining, sections were rinsed three times for 5 min in 1× PBS at room temperature and preincubated for 1 hr in antibody-blocking buffer that is 10% donkey serum in PBST (1× PBS with 0.3% Triton X-100). All rinses between incubation steps were with PBS. After rinsing, processed sections were incubated with different primary antibodies against collagen IV (Serotec; 1:100), Lamp-2 (Fitzgerald; 1:100), and podocalyxin (R&D Systems; 1:100) overnight in antibody-blocking buffer at 4°C. After three 10 min washes in 1× PBS at room temperature, sections were incubated with a donkey anti-rat, donkey anti-rabbit, and/or a goat anti-human secondary antibody conjugated to Alexa 488, 555, or 647 (Molecular Probes) for 2 hr at room temperature. All incubations were done under gentle agitation. After an intensive rinse with 1× PBS, sections were stained with DAPI, mounted with Dako Fluorescent Mounting Medium on glass slides, and a 0.17 mm coverslip was applied. Images were acquired using a Leica TCS SP5 confocal system using a HCX PL APO CS 40× 1.3 oil UV or a HCX PL APO LB 63× 1.4 oil UV objective. A zoom could have been used for some images. Deconvolution of confocal images was done using the Leica LAS-AF 3D Deconvolution tool. Imaris software was used to merge images, to perform 3D reconstruction, cross-sections, and movies. To quantify the fluorescence intensity corresponding to sFab or dFab constructs contained within the microvessels, we performed reconstruction of the microvessel network by recording at least 230 single optical layers (step size of 0.17 μm) with a HCX PL APO CS 40× 1.3 oil UV objective, at a 512 × 512-pixel resolution. The 15 min time point dFab sample was used to define optimal confocal settings with such settings used for the acquisition of all subsequent z stacks. Imaris software was used to reconstruct 3D images and to quantify the fluorescent signal contained in the microvessels by generating an Isosurface (default parameters including threshold of 25 for all images). All parameters were kept constant to allow comparative measurements between images. Three brain sections per condition were recorded with at least 600 μm of microvessels quantified per image. The fluorescence intensity/μm was calculated by dividing the total fluorescence intensity by the total length of microvessels measured. The average was calculated with Microsoft Excel, and statistical analysis (one-way ANOVA with Bonferroni's multiple comparison test) was performed using Prism.

For immunocytochemistry, bEnd3 cells seeded on 0.17 mm coverslips were carefully washed with warm PBS followed by a 10 min fixation with 3% paraformaldehyde. Coverslips were rinsed three times in 1× PBS at room temperature, preincubated for 5 min in PBST, followed by 30 min in 5% donkey serum in PBS. Primary and secondary antibodies are similar to those mentioned above. DAPI was used to label nuclei. Confocal scans were performed from the top to the bottom of the cell nucleus using a HCX PL APO CS 20× 0.7 dry UV objective or a HCX PL APO LB 63× 1.4 oil UV objective with a zoom of three, at a resolution of 512 × 512 pixels. dFab sample was used to establish the optimal confocal settings with such settings used for the acquisition of all subsequent z stacks (step size, 0.25 μm). Colocalization analysis was performed using the Imaris Colocalization tool. Briefly, confocal files were opened in Imaris, and the colocalization tool was activated with sFab or dFab as Channel A and Lamp-2 as Channel B. A threshold of 25 was used for both channels on all images. After building a colocalization channel, the percentage of lysosomes containing the sFab or dFab construct was obtained using the following value: percentage (%) of volume B above threshold colocalized = (NColoc/NObjectB) × 100. In total, three experiments with at least ten cells quantified per experiment were performed for each condition. The average was calculated with Microsoft Excel, and statistical analysis (one-way ANOVA with Bonferroni's multiple comparison test) was done in Prism.

Imaging and Quantification of Plaque Load

Fresh frozen brains from PBS-perfused animals were sagittal sectioned with a cryostat (CM3050S; Leica BioSystems) and processed for further analysis by

Figure 6. In Vivo Efficacy in a Chronic Study in Plaque-Bearing PS2APP Mice Treated by 14 Weekly i.v. Injections

Target plaque binding of administrated constructs bound to residual plaques at the end of the study is shown for low-dose mAb31, middose mAb31, low-dose sFab and middose sFab (A–D, respectively). Clear dose-dependent target occupancy is seen for sFab (C and D). Histological plaque distribution is shown for representative animals from baseline (E), vehicle (F), middose mAb31 (G), and middose sFab (H) groups. Reduction of plaques is clearly appreciable after treatment with middose sFab (H).

(I) Quantitative morphometric analysis after immunohistochemical staining of plaques is shown for cortex and hippocampus. Plaque load of untreated animals sacrificed at an age of 4.5 months is shown as baseline level of amyloidosis at the start of the study. A significant reduction in plaque numbers is evident after treatment with middose sFab compared to the progressive plaque formation seen in vehicle-treated animals; a trend of reduced plaque formation appears even at the low-dose sFab. Thus, sFab construct significantly reduces plaque numbers in both cortex and hippocampus.

(J) Analysis of plaque sizes revealed reduction of plaque numbers most pronounced for small plaque sizes.

Data are presented as mean ± SD. *$p \leq 0.05$, **$p \leq 0.01$, and ***$p \leq 0.001$. See also Figures S7 and S8.

immunofluorescence and quantitative morphometry essentially as described previously (Bohrmann et al., 2012) with some modifications. In this study, quantification of the plaque number in APPSwe/presenilin mice was obtained from six sections per mouse within the hippocampal formation and cortex and cut at a nominal thickness of 10 μm. After staining of sections with mAb31 at 2 μg/ml for 1 hr at room temperature and detection by affinity-purified goat anti-human IgG (H + L) conjugated to Alexa 555 at 20 μg/ml for 1 hr at room temperature (#A21433; Molecular Probes), virtual slides with a resolution of 0.645 μm/pixel were obtained with a Metafer4 slide scanner (MetaSystems). Quantitative image analysis was done by a customized rule set developed in-house for the automated detection of stained amyloid plaques after interactive selection within most affected brain regions using the Definiens XD 2.0 software package. Calculations were made with common spreadsheet software (Microsoft Excel). Statistical evaluation was done using a two-tailed Student's t test.

Flow Cytometry

For the intra- and extracellular TfR detection, bEnd3 cells were stained with an anti-CD71-Alexa 647 (YTA74.4) (AbD Serotec) or the IgG2a-Alexa 647 (G155-178) (BD PharMingen) isotype control. A goat-anti-human-Alexa 555 (Life Technologies) was used for the detection of the dFab and sFab constructs. A total of 1×10^6 cells was incubated for 1 hr at 4°C with the antibodies and washed twice with the staining buffer (BD PharMingen). For the intracellular staining, the cells were fixed (BD Cytofix) at 4°C for 30 min, permeabilized (BD Perm Buffer III) on ice for 30 min, and incubated with each antibody at 4°C for 1 hr. After staining, the cells were analyzed using a Guava easyCyte flow cytometer (Millipore).

In Vitro Transcytosis Assay

Medium and supplements for hCMEC/D3 (see Weksler et al., 2005) were obtained from Lonza. hCMEC/D3 cells (passages 26–29) were cultured to confluence in EBM2 medium containing 2.5% FBS, a quarter of the supplied growth factors, and fully complemented with supplied hydrocortisone, gentamycin, and ascorbic acid. For all transcytosis assays, high-density pore (1×10^8 pores/cm^2) PET membrane filter inserts (0.4 μm pore size, 12 mm diameter) were used in 12-well cell culture plates. The content of antibody in the samples was quantified using a highly sensitive IgG ELISA.

SUPPLEMENTAL INFORMATION

Supplemental Information includes Supplemental Experimental Procedures, eight figures, and one movie and can be found with this article online at http://dx.doi.org/10.1016/j.neuron.2013.10.061.

ACKNOWLEDGMENTS

We thank Professor Marco Celio for quantitative fluorescence determination (Frimorfo, Switzerland), Francoise Gerber and Krisztina Oroszlan for immunohistochemistry and confocal laser-scanning microscopy, Jürg Messer for quantitative morphometry, Ashley Hayes for cell culturing, Dieter Reinhardt for immunoassay measurements, and Claudia Baumgartner for in vitro transcytosis assay. We would also like to thank P.-O. Couraud, I.A. Romero, and B. Weksler for providing us with hCMEC/D3 cells. All authors are under paid employment by the company F. Hoffmann-La Roche.

Accepted: October 8, 2013
Published: January 8, 2014

REFERENCES

Bohrmann, B., Baumann, K., Benz, J., Gerber, F., Huber, W., Knoflach, F., Messer, J., Oroszlan, K., Rauchenberger, R., Richter, W.F., et al. (2012). Gantenerumab: a novel human anti-Aβ antibody demonstrates sustained cerebral amyloid-β binding and elicits cell-mediated removal of human amyloid-β. J. Alzheimers Dis. *28*, 49–69.

Crépin, R., Goenaga, A.L., Jullienne, B., Bougherara, H., Legay, C., Benihoud, K., Marks, J.D., and Poul, M.A. (2010). Development of human single-chain antibodies to the transferrin receptor that effectively antagonize the growth of leukemias and lymphomas. Cancer Res. *70*, 5497–5506.

Gosk, S., Vermehren, C., Storm, G., and Moos, T. (2004). Targeting anti-transferrin receptor antibody (OX26) and OX26-conjugated liposomes to brain capillary endothelial cells using in situ perfusion. J. Cereb. Blood Flow Metab. *24*, 1193–1204.

Kozik, P., Hodson, N.A., Sahlender, D.A., Simecek, N., Soromani, C., Wu, J., Collinson, L.M., and Robinson, M.S. (2013). A human genome-wide screen for regulators of clathrin-coated vesicle formation reveals an unexpected role for the V-ATPase. Nat. Cell Biol. *15*, 50–60.

Lakadamyali, M., Rust, M.J., and Zhuang, X. (2006). Ligands for clathrin-mediated endocytosis are differentially sorted into distinct populations of early endosomes. Cell *124*, 997–1009.

LaVaute, T., Smith, S., Cooperman, S., Iwai, K., Land, W., Meyron-Holtz, E., Drake, S.K., Miller, G., Abu-Asab, M., Tsokos, M., et al. (2001). Targeted deletion of the gene encoding iron regulatory protein-2 causes misregulation of iron metabolism and neurodegenerative disease in mice. Nat. Genet. *27*, 209–214.

Lesley, J., Schulte, R., and Woods, J. (1989). Modulation of transferrin receptor expression and function by anti-transferrin receptor antibodies and antibody fragments. Exp. Cell Res. *182*, 215–233.

Levy, J.E., Jin, O., Fujiwara, Y., Kuo, F., and Andrews, N.C. (1999). Transferrin receptor is necessary for development of erythrocytes and the nervous system. Nat. Genet. *21*, 396–399.

Liu, A.P., Aguet, F., Danuser, G., and Schmid, S.L. (2010). Local clustering of transferrin receptors promotes clathrin-coated pit initiation. J. Cell Biol. *191*, 1381–1393.

Matsui, T., Itoh, T., and Fukuda, M. (2011). Small GTPase Rab12 regulates constitutive degradation of transferrin receptor. Traffic *12*, 1432–1443.

Michel, V., Licon-Munoz, Y., Trujillo, K., Bisoffi, M., and Parra, K.J. (2013). Inhibitors of vacuolar ATPase proton pumps inhibit human prostate cancer cell invasion and prostate-specific antigen expression and secretion. Int. J. Cancer *132*, E1–E10.

Mielke, M.M., Wiste, H.J., Weigand, S.D., Knopman, D.S., Lowe, V.J., Roberts, R.O., Geda, Y.E., Swenson-Dravis, D.M., Boeve, B.F., Senjem, M.L., et al. (2012). Indicators of amyloid burden in a population-based study of cognitively normal elderly. Neurology *79*, 1570–1577.

Navaroli, D.M., Bellvé, K.D., Standley, C., Lifshitz, L.M., Cardia, J., Lambright, D., Leonard, D., Fogarty, K.E., and Corvera, S. (2012). Rabenosyn-5 defines the fate of the transferrin receptor following clathrin-mediated endocytosis. Proc. Natl. Acad. Sci. USA *109*, E471–E480.

Pardridge, W.M. (2012). Drug transport across the blood-brain barrier. J. Cereb. Blood Flow Metab. *32*, 1959–1972.

Pardridge, W.M., and Boado, R.J. (2012). Reengineering biopharmaceuticals for targeted delivery across the blood-brain barrier. Methods Enzymol. *503*, 269–292.

Paris-Robidas, S., Emond, V., Tremblay, C., Soulet, D., and Calon, F. (2011). In vivo labeling of brain capillary endothelial cells after intravenous injection of monoclonal antibodies targeting the transferrin receptor. Mol. Pharmacol. *80*, 32–39.

Poduslo, J.F., Curran, G.L., and Berg, C.T. (1994). Macromolecular permeability across the blood-nerve and blood-brain barriers. Proc. Natl. Acad. Sci. USA *91*, 5705–5709.

Richards, J.G., Higgins, G.A., Ouagazzal, A.M., Ozmen, L., Kew, J.N., Bohrmann, B., Malherbe, P., Brockhaus, M., Loetscher, H., Czech, C., et al. (2003). PS2APP transgenic mice, coexpressing hPS2mut and hAPPswe, show age-related cognitive deficits associated with discrete brain amyloid deposition and inflammation. J. Neurosci. *23*, 8989–9003.

Staquicini, F.I., Ozawa, M.G., Moya, C.A., Driessen, W.H.P., Barbu, E.M., Nishimori, H., Soghomonyan, S., Flores, L.G., 2nd, Liang, X., Paolillo, V.,

et al. (2011). Systemic combinatorial peptide selection yields a non-canonical iron-mimicry mechanism for targeting tumors in a mouse model of human glioblastoma. J. Clin. Invest. *121*, 161–173.

Sumbria, R.K., Zhou, Q.H., Hui, E.K., Lu, J.Z., Boado, R.J., and Pardridge, W.M. (2013). Pharmacokinetics and brain uptake of an IgG-TNF decoy receptor fusion protein following intravenous, intraperitoneal, and subcutaneous administration in mice. Mol. Pharm. *10*, 1425–1431.

Wang, D., El-Amouri, S.S., Dai, M., Kuan, C.Y., Hui, D.Y., Brady, R.O., and Pan, D. (2013). Engineering a lysosomal enzyme with a derivative of receptor-binding domain of apoE enables delivery across the blood-brain barrier. Proc. Natl. Acad. Sci. USA *110*, 2999–3004.

Weksler, B.B., Subileua, E.A., Perrière, N., Charneau, P., Holloway, K., Leveque, M., Tricoire-Leignel, H., Nicotra, A., Bourdoulous, S., Turowski, P., et al. (2005). Blood-brain barrier-specific properties of a human adult brain endothelial cell line. FASEB J. *19*, 1872–1874.

Yu, Y.J., Zhang, Y., Kenrick, M., Hoyte, K., Luk, W., Lu, Y., Atwal, J., Elliott, J.M., Prabhu, S., Watts, R.J., and Dennis, M.S. (2011). Boosting brain uptake of a therapeutic antibody by reducing its affinity for a transcytosis target. Sci. Transl. Med. *3*, 84ra44.